Crack Growth Rate Behaviour and Microstructural Features of Incoloy 800H under Fatigue and Creep-fatigue Conditions

D.Y. Seo[1], J. Tsang[1], R. Kearsey[1], W.J. Yang[2], K.S. Cho[2], J.H. Lee[2] and P. Au[1]
[1] *Institute for Aerospace Research, National Research Council Canada, Ottawa, Ontario, Canada ;*
[2] *Korea Institute of Materials Science, 531 Changwondaero, Changwon, Gyeongnam, Korea*
E-mail: *dongyi.seo@nrc-cnrc.gc.ca*

Abstract

Incoloy 800H is a solid-solution-strengthened iron-based austenitic alloy. In this study, the alloy was forged and solution heat treated followed by annealing at 982°C for three hours. Fatigue and creep-fatigue (10 and 30 second dwell) crack growth rate tests were performed using a fully automated DCPD technique to monitor crack growth. The results indicate that the growth rates of the creep-fatigue conditions are ten times faster than those of the fatigue condition at the same ΔK values. Similar crack growth rates between a 10 second and 30 second dwell was observed. The predominant fracture mode in both conditions was transgranular. Continuous stable oxides and oxide penetration due to internal oxidation associated with the chromium depleted zone were observed only in creep-fatigue crack growth rate tests. These microstructural features were observed a head of propagating creep-fatigue cracks, indicating that the faster crack propagation under creep-fatigue condition is likely to be a predominantly environment-assisted process. In particular, thicker oxide layers were observed in the creep-fatigue condition, as some of the strengthening phases such as MC or $M_{23}C_6$, were eliminated in the oxide region, reducing the resistance to crack growth.

Introduction

Incoloy 800H alloy is an austenitic alloy with average grain size greater than ~70μm. It is a solid-solution-strengthened alloy with additional strengthening by titanium nitrides and carbides such as MC and $M_{23}C_6$. This alloy has been broadly used in furnace components and equipment, petrochemical furnace cracker tubes, pigtails and headers, and sheathing for electrical heating elements due to its high creep rupture strengths, and resistance to high temperature corrosion [1]. Alloy 800H has been selected as one of the potential candidate alloys for Generation IV nuclear plants [2]. In these applications, the alloy may be exposed to continuous loading, cyclic loading, or then combinations at elevated temperatures. Previous studies investigated the damage mechanisms of Alloy 800H at elevated temperature under fatigue, creep, and creep-fatigue conditions [3,4,5]. However, the investigations focused on low cycle fatigue behaviour at 600 and 750°C or crack growth behaviour at 650°C. There are not very little data available for crack

growth behaviour at 750°C under fatigue and creep-fatigue conditions. In this study, the forged Incoloy 800H alloy was solution heat treated and annealed. The crack growth behaviour of the heat treated Incoloy 800H under fatigue and creep-fatigue conditions was elucidated in terms of microstructural features.

Materials, Specimens and Experimental Procedures

The nominal composition of Incoloy 800H is listed in Table 1 [4]. The material was forged and then solution heat treated at 1150°C for 4 hours, followed by air cooled. The solution heat treated alloy was subsequently annealed at 982°C (heating rate: 80°C/hour) for 3 hours and air cooled. Compact tension, C(T), specimens were machined from the forged and heat treated alloy based on reference [6].

Table 1. Nominal composition of Incoloy 800H (wt%) [4]

Al	C	Cr	Cu	Fe	Mn	Ni	S	Si	Ti
0.3	0.08	21.3	0.15	balance	0.74	33.8	<0.002	0.55	0.36

Prior to testing, the C(T) specimen side surfaces were mechanically polished to achieve a mirror finish and to facilitate surface crack length verification. The specimens were then ultrasonically cleaned and their dimensions were measured. For microstructural analysis, small pieces were cut from the forged or heat treated Incoloy 800H and were metallographically prepared using standard procedure. After polishing, the specimens were etched using a solution (Glyceregia) of 10 ml HNO_3+ 50ml HCl + 30 ml glycerin. In addition, once testing was completed, the cross sections as well as the fracture surfaces of selected samples were examined using an optical microscope and a Phillips XL 30S scanning electron microscope (SEM) with energy dispersive spectroscopy (EDS).

Table 2. Test conditions of fatigue and creep-fatigue crack growth rate tests.

	Hold-Time (seconds)	Frequency (Hz)	Temperature (°C)	Load ratio (R)
FCGR Test	0	10	750°C	+0.1
CFCGR Test	10	0.07692	750°C	+0.1
CFCGR Test	30	0.03333	750°C	+0.1

The fatigue crack growth rate (FCGR) and creep-fatigue crack growth rate (CFCGR) tests at 750^{o}C were performed on a MTS model 305.03 servo-hydraulic test machine in accordance with the guidelines set in ASTM E647 [6]. The test comprised of three stages: (1) Fatigue Pre-cracking, (2) K-decreasing (Load Shedding), and/or (3) K-increasing with a constant load, K-increasing with a 10 second dwell (creep-fatigue) or K-increasing with a 30 second dwell (creep-fatigue). A Fracture Technology Associates (FTA) Series 2001 automated fatigue crack growth system was utilized to control the test and a direct current potential

difference (DCPD) technique was applied to monitor the changes in crack size with respect to the number of cycles. Table 2 shows all of the test conditions. For the FCGR and the pre-cracking segment of the CFCGR tests, a sinusoidal force function (at a frequency rate of 10 Hz) was used. For the CFCGR K-increasing segments, a custom waveform was created, which includes a 1.5 second linear ramp from the minimum to maximum force level, a dwell time of either 10 or 30 seconds at the maximum force level, and a 1.5 second linear ramp down from the maximum to minimum load, for a total duration of 13 or 33 seconds. It should be noted that the K-decreasing segment was not performed for the CFCGR tests.
After the tests, the differences between the visually measured crack size and the DCPD crack size was corrected using a linear correction factor as recommended in references [6,7]. The ΔK values for the C(T) specimen were calculated using the solution provided in Annex A1 of the ASTM E647 [6]. In addition, the specimen size requirement in reference [6] was also verified during the post-test analysis.

Results and Discussion

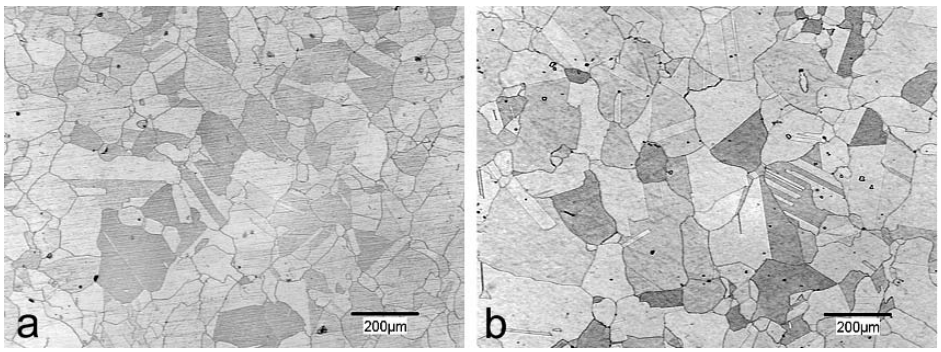

Figure 1 Optical micrographs of Incoloy 800H (a) in as-forged condition and (b) after the heat treatment.

Figure 1 shows optical micrographs of the samples before and after heat treatment. In the forged condition, grains were finer compared to the heat treated condition and twinning was often observed. After heat treatment, the grains coarsened to about 200 μm in size and some twinning was still observed. It was observed that the grain boundary morphology was planar in both conditions. Detailed microstructural analysis using a SEM with EDS was also conducted. As shown in Figure 2a, particles with a diameter of about 20 μm were often observed in the forged sample. EDS analysis indicates that these particles contain C, N, Hg, and

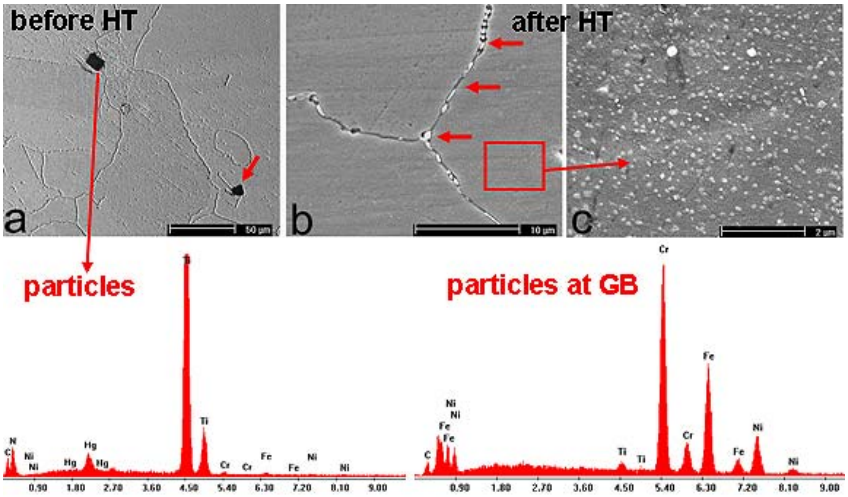

Figure 2. SEM micrographs of Incoloy 800H before (a) and after (b,c) heat treatment. EDS spectrums of particles in (a) and at grain boundaries in (b) are shown below the SEM micrographs.

Ti. In particular, the amount of C and Ti is relatively high compared to that in the matrix. These particles are likely to be Ti-carbides or Ti-nitrides containing some impurities. The nitrides are stable at all temperatures below the melting point and are, therefore, unaffected by heat treatment [1]. After the heat treatment, fine particles at the grain boundaries as well as very fine precipitates within the grains were frequently observed as shown in Figures 2b. From the EDS analysis, the particles at the grain boundaries are different from the particles in Figure 2a. These grainboundary particles have a high Cr and C content with Fe (see EDS spectrum in Figure 2b). A previous study indicates that chromium carbides are precipitated in the alloy at temperatures between 540 and 1095°C [1]. Other studies also suggested that the carbides were identified as $M_{23}C_6$ type precipitates (M= Cr, Fe) [8,9]. Therefore, the particles at the grain boundaries are likely to be chromium carbides and iron carbides. From the results reported previously [8,9,10], it is also speculated that the very fine intragranular precipitates are likely to be MC type carbides. However, transmission electron microscopy (TEM) analysis is required to verify the nature of these fine precipitates.

Figure 3 shows the fracture morphology in the K-decreasing and K-increasing transition region of specimens tested with 0 and 10 sec dwell. In the K-decreasing region (right side of Figure 3a), the fracture surface is relatively smooth, whereas in the K-increasing (left side of Figure 3a), the fracture surface morphology is predominantly transgranular and characterized by river patterns that are often associated with pure fatigue loading conditions. Figure 3b shows the fracture surface in the K-increasing region

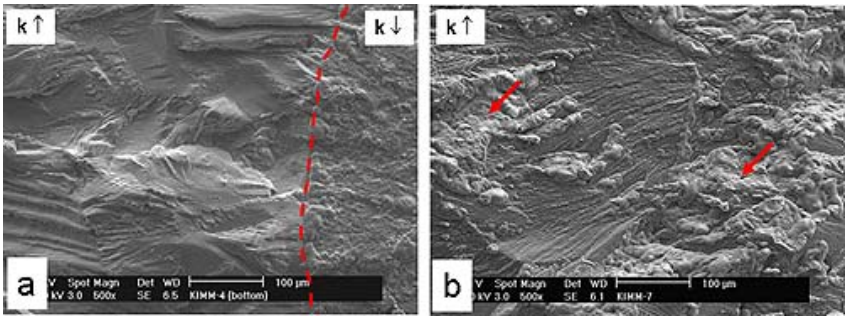

Figure 3. SEM images of fracture surface after (a) fatigue and (b) creep-fatigue crack growth rate tests (10 sec dwell). Dotted line represents transition of K-decreasing on the right side of photo, to K-increasing on the left side of photo.

after a creep-fatigue crack growth test with a 10 sec dwell. The fracture surface was similar to the surface observed in the K-increasing condition with no dwell except for the surface oxides (see arrows in Figure 3b) formed on the fracture surface. In the creep-fatigue crack growth rate test with a 30 sec dwell, a similar fracture surface was also observed. Overall, the fracture surfaces between the fatigue and creep-fatigue tests are relatively similar. It is also confirmed that transgranular crack propagation is the major mode of crack propagation for both the fatigue and creep-fatigue crack growth rate tests as shown in Figure 4. There was no indication of the formation of creep cavities in the creep-fatigue crack growth test. However, thick oxides were observed on the fracture surfaces in specimens tested with 10 and 30 sec dwell. This is probably due to the grain boundary strengthening by the fine particles at grain boundaries, shown in Figure 2b.

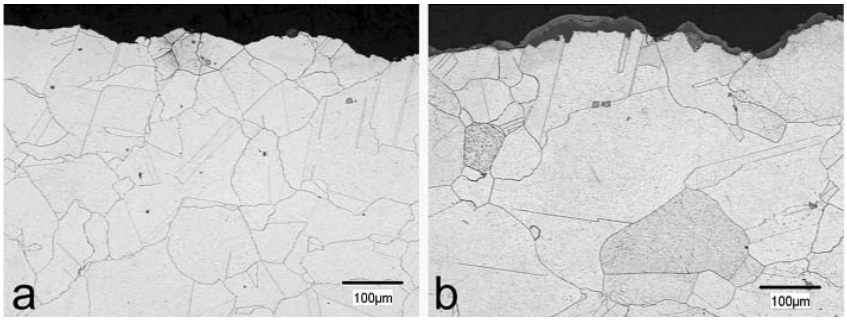

Figure 4. OM images of cross sections of fracture surface after (a) fatigue- and (b) creep-fatigue crack growth rate tests (30 sec dwell).

Figure 5 shows backscattered electron (BSE) images of the cross sections of the samples in the K-increasing region of samples tested with and without dwell. In particular, much thicker oxides (>10μm) were formed periodically in the samples tested with 10 and 30 sec dwell compared to the sample with no dwell as shown in Figure 5.

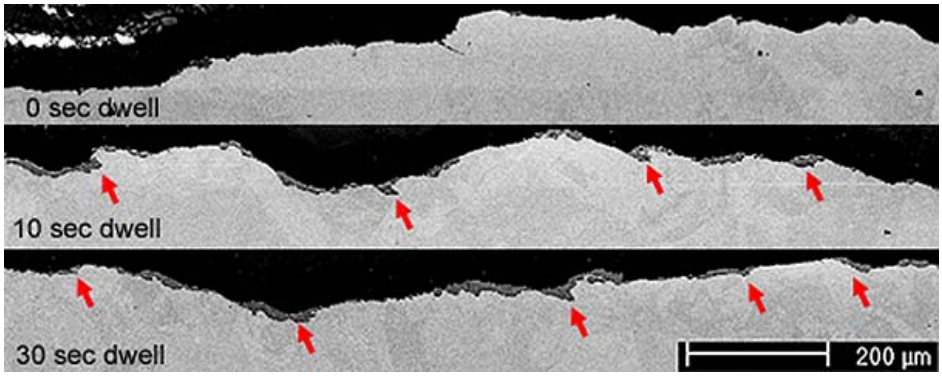

Figure 5. BSE images of the K-increasing regions in fatigue and creep-fatigue crack growth rate tests. Short arrows indicate the penetration of oxides.

Detailed features of the oxides are shown in Figure 6. In the case of the sample tested with no dwell in Figures 6a and b, thin oxides were formed and appear not adhere well on the surface, whereas in the samples tested with 10 and 30 sec dwell the oxides were adherent, compact, dense and continuous, in Figures 6c, d, e and f. It is noted that the thick oxides appear to have formed easily near grain boundaries as shown in Figure 6c (dotted lines are grain boundaries). Penetration of the oxides into the alloy was also often observed in the samples tested with dwell in Figures 5 and 6e. These features likely indicate internal oxidation. As mentioned previously, chromium and iron carbides precipitates were observed at grain boundaries in the heat treated condition.

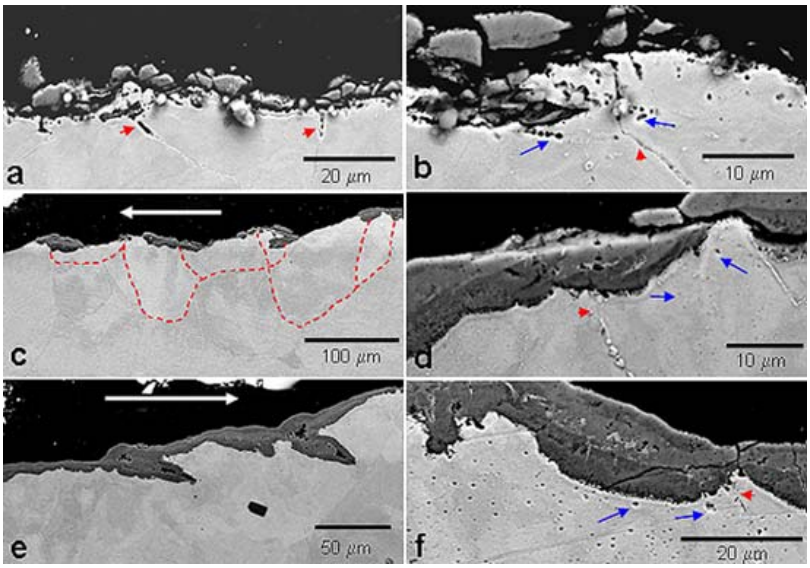

Figure 6. BSE images of the cross sections: (a and b) fatigue crack growth rate test, (c and d) creep-fatigue crack growth rate test with 10 sec dwell, and (e and f) creep-fatigue crack growth rate test with 30 sec dwell. Short arrows indicate the absence of precipitates at grain boundaries near surface oxides. Long arrows indicate voids formed near the oxides. Long white arrows in (c and e) show direction of crack propagation.

However, these precipitates disappeared where the thick oxides were formed as indicated in Figures 6a, b, d and f (see short arrows in the figures).

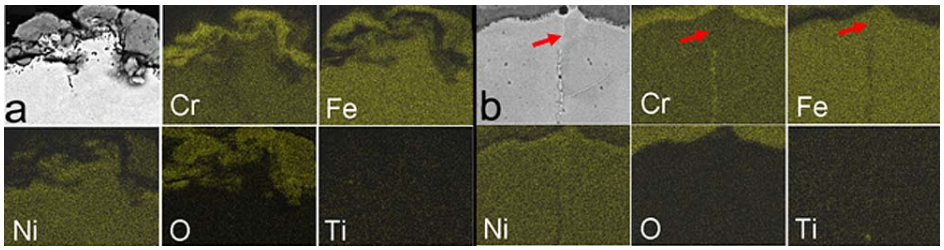

Figure 7. EDS elemental mappings of the cross section of the tested samples in (a) fatigue and creep-fatigue crack growth rate test with (b) 30 sec dwell conditions. Arrows show the absence of precipitates at grain boundary.

EDS-mapping analysis in Figure 7 confirms that the surface oxides are consisted of chromium, nickel and iron oxides. It is noted that chromium oxide formed close to the alloy and nickel and iron oxides formed on the top of the chromium oxide. It is suggested that the formation of these oxides led to disappearance of the chromium and iron carbides in the vicinity, in Figures 7b (see arrows). These oxides were formed via outward diffusion of Cr, Ni and Fe during testing at 750°C. Previous studies indicated that Incoloy 800H forms a double layer oxide that consists of an outer layer of Fe_2O_3 or Fe_3O_4, and an inner layer of Cr_2O_3 [11]. Therefore, it is speculated that the same occurred in current work. In addition, the nickel oxides between Cr_2O_3 and Fe_2O_3 or Fe_3O_4 in Figure 7b are likely to be identified as $NiFe_2O_4$ as reported in [12]. The presence of nickel oxide could be an indication of the internal oxidation mentioned earlier.

The crack growth rates versus stress intensity range (ΔK) curves are shown in Figure 8. As expected, the introduction of a 10 sec and a 30 sec dwell increase the crack growth rate. The creep-fatigue data was limited due to the low strength of the Incoloy 800H alloy at 750°C. Yield strength and UTS of the heat treated Incoloy 800H at 750°C are 146 and 229 MPa [13], which is lower than those in reference [1]. As shown in Figure 8a, the FCGR data for the K-decreasing and K-increasing (with no dwell time) segments are in very good agreement with each other and provide a consistent baseline for comparison with the creep-fatigue tests. The growth rates of the creep-fatigue specimens are an order of magnitude greater than that of the FCGR at the same ΔK values. It can be seen that the slope of the Paris Regime of the FCGR and CFCGR curves are similar as shown in Figure 8b, which shows that the slopes range from 2.6 to 3.4 according to the Paris' equation. The crack growth rates of the specimens with a 10 and 30 second dwell are very similar as shown in Figures 8a and b. This suggests that the oxidation kinetics of Incoloy 800H is very sensitively rapid at 750°C and oxidation damage saturates quickly and dominates the crack growth behaviour. It is noted that the formation of continuous stable oxides as well as internal oxidation occurred only in CFCGR specimens, as shown in Figures 5, 6, and 7. Especially thicker inner layer of Cr_2O_3 in the creep-fatigue condition was formed compared to those for the FCGR

specimens. Osgerby reported that in Incoloy 800, as the chromium level is reduced, the amount of the strengthening phases is reduced with $M_{23}C_6$ going into solution at the elevated temperatures at the 10%Cr level [14]. A similar reduction in γ′ precipitate is also observed with the solvus temperature reduced from ~750°C in the original alloy to ~700°C at the 10%Cr level [14]. This suggests that subsurface zone depleted in chromium formed during oxidation of the alloy and these zones are weaker than the original alloy due to the reduction of the main strengthening phase. In Incoloy 800H, continuous thick oxides and oxide penetration due to internal oxidation associated with the chromium or iron depleted zone were observed only in creep-fatigue crack growth rate tests, as some of the strengthening phases such as MC or $M_{23}C_6$, were eliminated in the oxide region, reducing the resistance to crack growth. These microstructural features were observed a head of propagating creep-fatigue cracks, indicating that the faster crack propagation under creep-fatigue condition is likely to be a predominantly environment-assisted process. Therefore, it is expected that subsequent tests with the same dwell times under vacuum would provide very benefit.

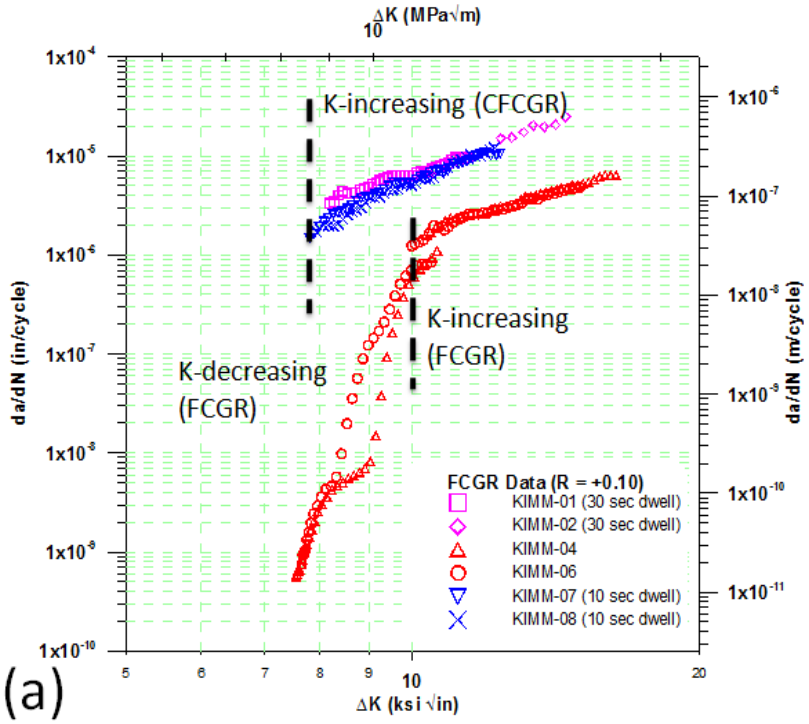

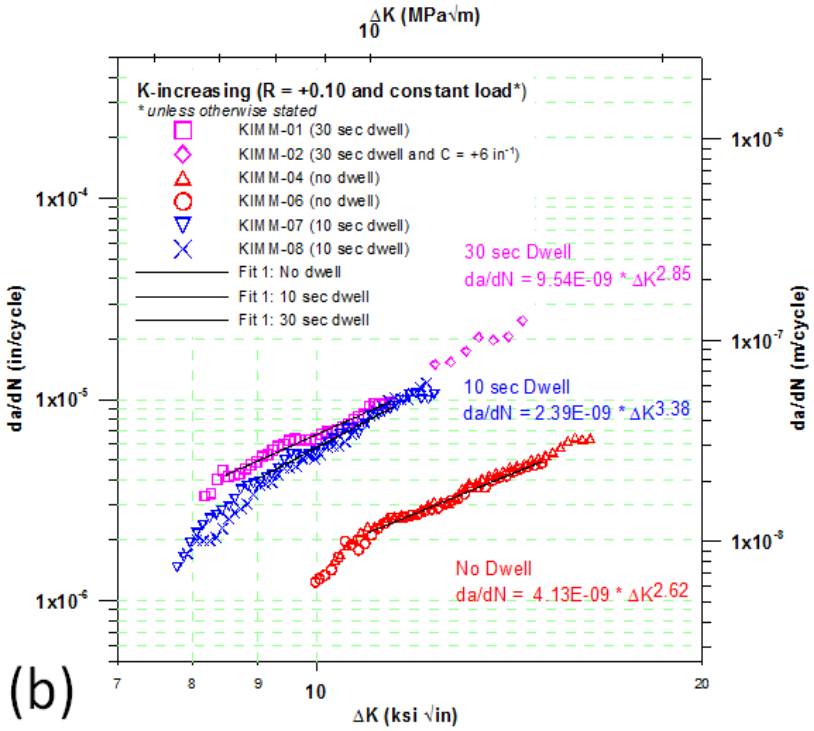

Figure 8. (a) Crack growth rate per cycle vs stress intensity factor for fatigue and creep-fatigue specimens and (b) K-increasing crack growth rate per cycle vs stress intensity factor for fatigue and creep-fatigue specimens with curve fitting.

Conclusion

Incoloy 800H alloy was forged and solution heat treated followed by annealing at 982°C for three hours. Microstructure of the heat treated alloy shows that the particles at the grain boundaries are likely to be chromium carbides and iron carbides. It is also speculated that the very fine intragranular precipitates, probably MC type carbides, are formed. Fatigue and creep-fatigue (10 and 30 second dwell) crack growth rate tests were performed using a fully automated DCPD technique. The results indicate that the growth rates of the creep-fatigue conditions are an order of magnitude greater than those of the fatigue condition at the same ΔK values. Similar crack growth rates between a 10 second and 30 second dwell was observed, indicating that those dwell times are approaching the saturation point. The predominant fracture mode in both conditions was transgranular. Microstructural analysis indicated that continuous thick oxides such as Fe_2O_3 or Fe_3O_4 and Cr_2O_3 as well as oxide penetration due to internal oxidation were observed only in creep-fatigue crack growth rate tests. In particular, thicker Cr_2O_3 layer was observed in the creep-fatigue condition and resulted in the formation of chromium depleted zone, which is associated with the higher crack growth rate because main strengthening phases such as MC or $M_{23}C_6$ are eliminated near the oxides.

References

1. Incoloy alloy 800H and 800HT, Special Metals, www.specialmetals.com.
2. Next generation nuclear plant materials research and development program plan, INEEL/EXT-04-02347, Idaho National Engineering and Environmental Lab., Bechtel BWXT Idaho, LLC, Idaho Falls, Idaho, Spet. 2004.
3. J.O. Nilsson, and T. Thorvaldsson, Low cycle fatigue behaviour of alloy 800H at 600C-effect of grain size and g'-precipitate dispersion, Fatigue Frat. Engng Mater. Struct., Vol 8, No. 4, pp. 373-384, 1985
4. K.Y. Hour and J.F. Stubbins, The effects of hold time and frequency on crack growth in alloy 800H at 650C, Metall. Trans. A, Vol. 20A, Spet. 1989, pp 1727-1734.
5. Z. Mu, K. Bothe and V. Gerold, Damage mechanism in alloy 800H under creep-fatigue conditions, Fatigue Frat. Engng Mater. Struct., Vol 17, No. 5, pp. 523-537, 1994.
6. Standard Test Method for Measuring Fatigue Crack Growth Rates, American Society for Testing and Materials (ASTM) E647-05.
7. K. Donald, Automated Fatigue Crack Growth Analysis – Series 2001 User's Reference Manual, Version 3.03.02, Fracture Technology Associates, Bethlehem, PA, USA, 2003.
8. K. Bhanu Sankara Rao et al.,On massive carbide precipitation during high temperauture low cycle fatigue in alloy 800H, Scripta Met., Vol 31, No 4, 1994, pp. 381-386.
9. Viktor Guttmann and Jens Timm, On the influence of the thermal pretreatment on creep and microstructure of alloy 800H, Z Metallkd, vol. 81, No. 6, 1990, pp. 428-432.
10. J.A. Todd and J. Ren, The effect of cold work on the precipitation kinetics of an advanced austenitic steel, Mater. Sci. Eng. A, 117, 1989, pp. 235-245.
11. J.C. Langevoort et al., On the oxide formation on stainless steels AISI 304 and Incoloy 800H investigated with XPS, Applied Surface Science, 28, 1987, pp. 167-179.
12. L. Tan et al., Effect of shot-peening on the oxidation of alloy 800H exposed to supercritical water and cyclic oxidation, Corrosion Science, accepted manuscript, 2008.
13. Private communication with KIMM 2007.
14. S. Osgerby, Development of de-alloyed zone during oxidation: effects on microstructure and spallation behaviour, Materials Science and Technology, Vol. 16, October, 2000, pp. 1233- 1236.